SANDIA REPORT

SAND2014-1978
Unlimited Release
Printed March 2014

Modeling of ESD Events from Polymeric Surfaces

Kent B. Pfeifer

Prepared by
Sandia National Laboratories
Albuquerque, New Mexico 87185 and Livermore, California 94550

Sandia National Laboratories is a multi-program laboratory managed and operated by Sandia Corporation, a wholly owned subsidiary of Lockheed Martin Corporation, for the U.S. Department of Energy's National Nuclear Security Administration under contract DE-AC04-94AL85000.

Sandia National Laboratories

Issued by Sandia National Laboratories, operated for the United States Department of Energy by Sandia Corporation.

Printed in the United States of America. This report has been reproduced directly from the best available copy.

Available to DOE and DOE contractors from
U.S. Department of Energy
Office of Scientific and Technical Information
P.O. Box 62
Oak Ridge, TN 37831

Telephone:	(865) 576-8401
Facsimile:	(865) 576-5728
E-Mail:	reports@adonis.osti.gov
Online ordering:	http://www.osti.gov/bridge

Available to the public from
U.S. Department of Commerce
National Technical Information Service
5285 Port Royal Rd.
Springfield, VA 22161

Telephone:	(800) 553-6847
Facsimile:	(703) 605-6900
E-Mail:	orders@ntis.fedworld.gov
Online order:	http://www.ntis.gov/help/ordermethods.asp?loc=7-4-0#online

SAND2014-1978
Unlimited Release
Printed March 2014

MODELING OF ESD EVENTS FROM POLYMERIC SURFACES

Kent B. Pfeifer
Microsystems Enabled Detection, 1716
B61-12 Integrated Systems Design, 2152
Sandia National Laboratories
P.O. Box 5800
Albuquerque, NM 87185-1425

Abstract

Transient electrostatic discharge (ESD) events are studied to assemble a predictive model of discharge from polymer surfaces. An analog circuit simulation is produced and its response is compared to various literature sources to explore its capabilities and limitations. Results suggest that polymer ESD events can be predicted to within an order of magnitude. These results compare well to empirical findings from other sources having similar reproducibility.

CONTENTS

Modeling of ESD Events from Polymeric Surfaces 3
1. Introduction [Begin Sections on odd pages] 7
Theory 9
    Charge Transfer 9
    Validation 16
Circuit Model 17
    Rationale 17
    Numerical Approach 19
Final Model 23
3: Conclusion 24
4: Appendix A: Sample Laplace Inverse program 26
5. References 28
Distribution 31

FIGURES

Figure 1: Figure showing regions of damage in a typical semiconductor for various voltages and currents. 7

Figure 2: Figure illustrating the relationships between the dimensions and the electric fields for a charged polymer placed between a set of ground elements. 8

Figure 3: Plot of charge transfer efficiency as a function of height from ground plane for charged polymer. 9

Figure 4: Distributed model of a lossy waveguide showing a differential length of guide with associated resistance, capacitance, conductance, and inductance per unit length. 10

Figure 5: Plot of transient current data from ESD discharge on 50 cm x 50 cm x 6 mm PVC plate charge to a surface density of 10μC/m^2 and discharged into a 20mm diameter grounded metal sphere. 13

Figure 6: Plot of the solution using $R'C'=2x10^{-3}$ s/m^2 of Eq. [14] overlayed with data from Horenstein, Davidson, and Mueller suggesting general agreement between the theory and experimental data.[6,13,14,15] 11

Figure 7: Plot of calculated charge vs. measured charge for several ESD experiments reported in literature from low-conductivity polymers using 10 mm radius grounded electrodes 15

Figure 8: Illustration showing Thévenin equivalent of the low-conductivity surface ESD simulation circuit where *f(s)* and *g(s)* are defined in Eq.[19]. 18

Figure 9: Equivalent circuit model of ESD from a polymer sheet charged to a surface voltage that provides an equivalent Q'_o as found in Eq. [17] 17

Figure 10: Proposed circuit model of ESD from a polymer sheet charged to a surface voltage that provides an equivalent Q'_o as found in Eq. [17]. 19

Figure 11: Plot of transient discharge data from literature (black line) compared to solution of the model of Eq. [18] (dashed line) 20

Figure 12 Plot of transient discharge data from literature (thin line) compared to solution of the model of Eq. [18]. 22

Figure 13: Plot of three simulations from the Dinallo[8] data showing the variation in the response that can occur in the charging and the ESD from selected polymers. 23

1. INTRODUCTION

The detrimental effects of electrostatic discharge (ESD) on sensitive electronic circuits is well

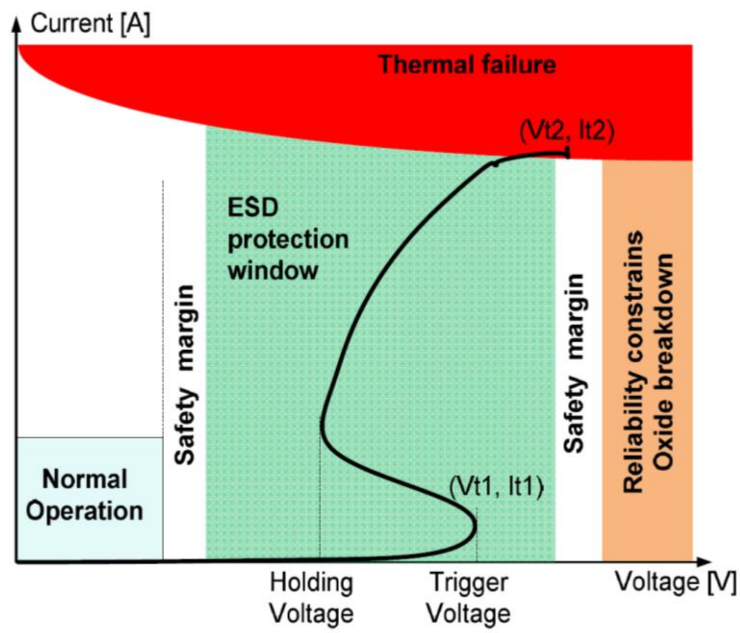

Figure 1: Figure showing regions of damage in a typical semiconductor for various voltages and currents. Diagram illustrates how excess voltage and current due to electrostatic discharge events leads to different types of damage depending on duration and magnitude of the event. Solid line shows I-V curve for an ESD protection device.[1]

known and strategies to eliminate ESD effects are important considerations in new circuit designs. A significant amount of research has been devoted to reducing the mechanisms of damage in circuitry by including ESD damage reduction structures (ESD protection diodes) in the design of high-density CMOS circuitry as well as implementation of engineered controls on the handling of such devices by using electrostatic discharge safe wrist straps, bench covers, and conducting surfaces on floors and other laboratory surfaces.[1, 2, 3, 4]

Damage from ESD events can occur due to two mechanisms that may or may not be evident immediately in the performance of the affected circuit. The first being absolute magnitude over-voltage spikes that can cause structural breakdown of thin insulators such as oxide layers in CMOS transistors. This is represented by the tan region in Figure 1 and can lead to latent defects appearing in the performance of the system. Full or partial oxide breakdown can cause catastrophic failure of the part by shorting the gate to the source or drain of the device or can produce a more subtle change such as a shift in the threshold voltage of the part that may reduce the reliability but not be immediately evident in the overall performance. The second main failure mechanism is caused by an overcurrent event in a circuit that can lead to localized heating of parts that leads to layers being shorted via ablation events or pyrolization carbonation and subsequent failure of the part.

We attempt to quantify and define a predictive model of electrostatic discharge from charged polymer surfaces that is useful to design subsystems with adequate ESD protection, but are

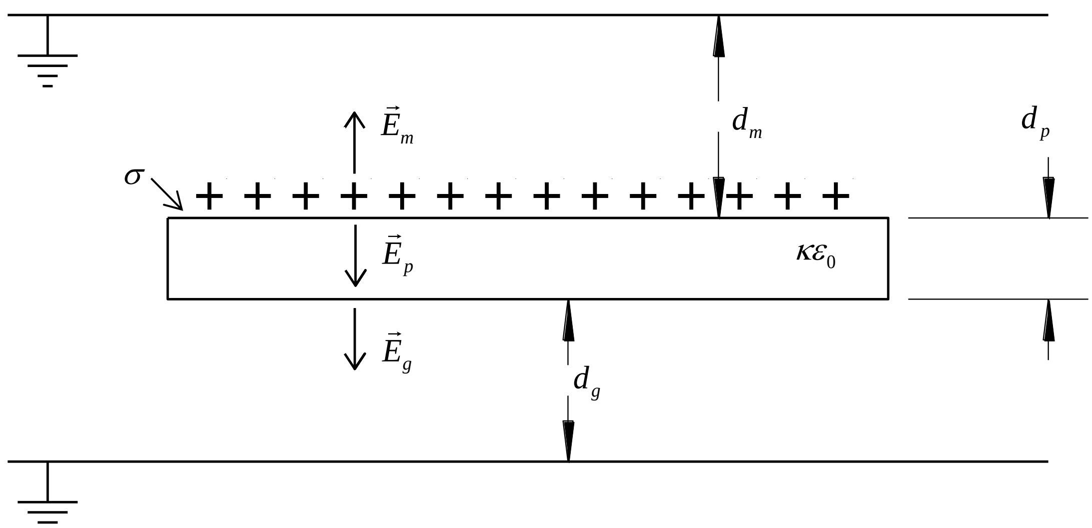

Figure 2: Figure illustrating the relationships between the dimensions and the electric fields for a charged polymer placed between a set of ground elements.

designed within traceable, defendable constraints. We also attempt to define an analog circuit model that can be used as a source term for simulation of ESD events from polymer surfaces. The model is defined and characterized against several literature studies to validate it and explore its capabilities and limitations.

THEORY

Charge Transfer

The total charge released from triboelectrically charged polymers is highly dependent on several factors including the dielectric constant, the thickness of the material, its location with respect to

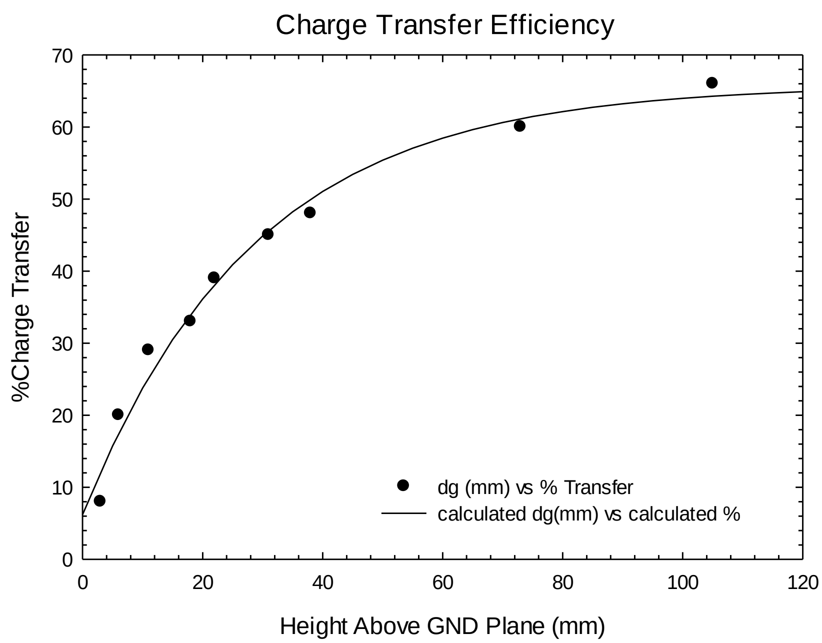

Figure 3: Plot of charge transfer efficiency as a function of height from ground plane for charged polymer.

ground planes, the geometry of the probe, the charge density on the surface of the polymer, material properties of surrounding structures, and the temperature and humidity of the environment. Construction of a predictive theory of electrostatic discharge (ESD) from a polymer surface requires the ability to relate the electrostatic voltage on the polymer with respect to the local ground to the total charge transferred to a probe element such as a cable or pin on a connector. All geometrical relationships will be described with respect to Figure 2.

Assuming a uniform charge density (σ), the electric fields emanating from the surface of the polymer block are given by the standard electromagnetic relationship:

$$\sigma = \varepsilon_0 E_m + \kappa\varepsilon_0 E_p \qquad [1]$$

Equation [1] describes the discontinuity between the electric field above the surface of the polymer and the electric field in the polymer due to the surface charge density (σ) on the polymer as derived from Gauss' Law.[5] The electric field measured above the polymer is called $\vec{E}_m$, the electric field in the polymer is $\vec{E}_p$, and the dielectric constant of the polymer is κ. The location of the polymer with respect to the ground planes and its thickness are given as d_m, d_g, and d_p respectively. Additionally, ε_o is the permittivity of free space (8.85×10^{-12} *F/m*). Assuming no net charge on the bottom of the polymer, the relationship between E_p and E_g is given below.

$$0 = \kappa\varepsilon_0 E_p - \varepsilon_0 E_g \qquad [2]$$

If we write Kirchhoff's voltage law around the circuit while ignoring the fringing fields we obtain the following relationship:

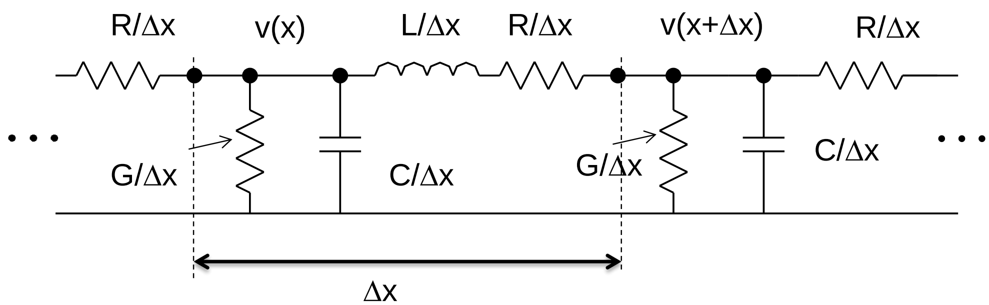

Figure 4: Distributed model of a lossy waveguide showing a differential length of guide with associated resistance, capacitance, conductance, and inductance per unit length.

$$d_m E_m = d_g E_g + d_p E_p \qquad [3]$$

Rearranging Eqs.[1], [2], and [3] leads to an expression between the electric field at the surface of the polymer and the observable surface charge density.[6,7]

$$\sigma = \varepsilon_o E_m \left(1 + \frac{\kappa d_m}{d_p + \kappa d_g}\right) \qquad [4]$$

The charge density (Eq. [4]) is related to the material properties of the polymer and the location of the polymer with respect to ground. Note that in the limits of d_m=0, Eq. [4] reduces to the standard relationship between surface charge density and electric field, and in the limit of $d_g \rightarrow \infty$, we arrive at the same relationship. However, for values of d_m and d_g in between, values of σ can be larger than $\varepsilon_o E_m$. Thus, depending on the geometry of the problem, σ can be larger than the standard Gaussian limit of 26.6 μC/m^2 value quoted in the literature for air breakdown ($\varepsilon_o E_m$=(8.85x10^{-12} F/m x 3 MV/m)= 26.6 μC/m^2).[6]

A common attribute of the polymers of interest is their extremely low conductivity. Engineers use a standard technique for measurement of potential from a non-conducting surface. This technique is to employ an instrument called an electrostatic voltmeter that employs a large area conducting plate assumed to be one element of a capacitor located at a precise distance (d_m) above the surface to be measured to find the electric field in the spatial interval. The surface potential (V_f) is then inferred from the known distance and the measured field. Thus, Eq. [4] can be modified to find the charge density in terms of published potentials for triboelectric charging of the polymers.[8]

Because of the low conductance of the polymer, charge on the surface of the polymer is essentially immobile. Thus, during a discharge event, charge moves inward radially as charge is removed. For example, a grounded probe that approaches the surface of the polymer will be capacitively coupled to the charge layer and at a certain distance, charge will transfer via an effective RC circuit to the probe. However, since charge is immobile on the surface, charge

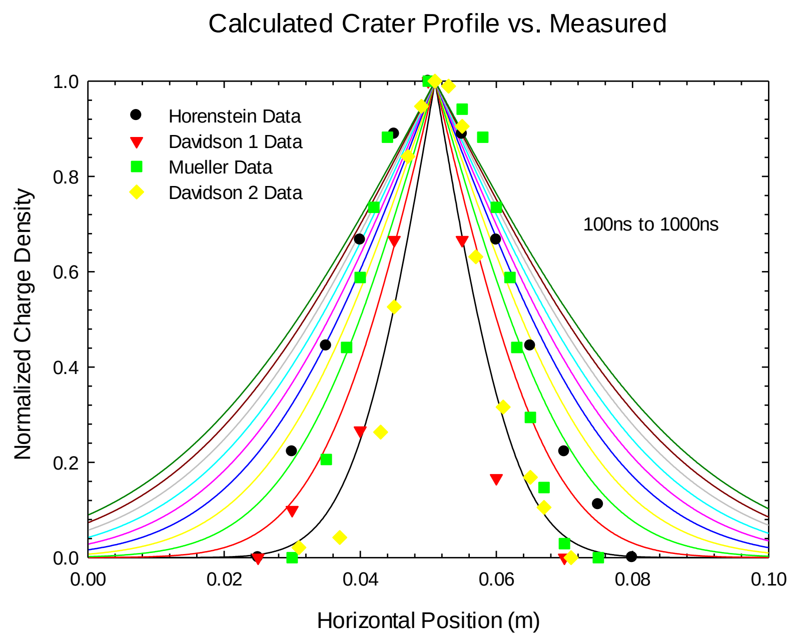

Figure 5: Plot of the solution using *R'C'=2x10^{-3} s/m^2* of Eq. [14] overlayed with data from Horenstein, Davidson, and Mueller suggesting general agreement between the theory and experimental data.[6,13,14,15] Data are normalized due to differing initial surface charge densities in the various experiments.

cannot move inward to replace that which was transferred until the local electric field becomes equivalent to the air break-down field which is considered to be approximately 3 MV/m. When this occurs, charge moves radially inward until there is a state reached where the fields are all below the breakdown field amplitude. Davidson *et al* have mapped the region of disturbed charge as a function of proximity of ground planes and have shown that for a given geometry, a transfer efficiency (Figure 3) can be measured and a characteristic area (ΔA) of charge transfer can be found. Experimentally, for polystyrene, this is found to be about ΔA=6.4x10^{-3} m^2 or a circular area with radius of 45 mm.[6] We are suggesting an average area with a diameter on the order of 45 mm; however, measurements found in literature range from diameters of around 30 mm to around 60 mm implying an uncertainty in the standard area of about ±5x$10^{-3}$$m^2$. For our purposes, order of magnitude is adequate. This 45 mm radius is also found to be consistent with values calculated in the literature.[9] Naturally, the question arises as to why a "standard area" should exist and be the same for all of the good dielectrics that have been considered. We can obtain a plausible explanation if we consider the circular region of charge depletion as a lossy waveguide structure.

A differential length of waveguide (*Δx*) where we define the resistance per unit length (*R'=R/Δx*), the capacitance per unit length (*C'=C/Δx*), the conductance per unit length (*G'=G/Δx*), and the inductance per unit (*L'=L/Δx*) as is shown in Figure 4. We can write loop equations for the current around the loop and the voltage across the differential length of waveguide as follows:

$$\begin{aligned} &v(x)-v(x+\Delta x)-L\frac{di}{dt}-R\,i=0 \\ &i(x)-i(x+\Delta x)-Gv(x+\Delta x)-C\frac{dv(x+\Delta x)}{dt}=0 \end{aligned} \qquad [5]$$

If we then divide by *Δx*, rearrange the equations, and take the limit as *Δx* approaches zero, we arrive at the following partial differential equations.

$$\begin{aligned} &\lim_{\Delta x\to 0}\left[\frac{v(x)-v(x+\Delta x)}{\Delta x}-\frac{L}{\Delta x}\frac{di}{dt}-\frac{R}{\Delta x}i\right]=0 \\ &\lim_{\Delta x\to 0}\left[\frac{i(x)-i(x+\Delta x)}{\Delta x}-\frac{G}{\Delta x}v(x+\Delta x)-\frac{C}{\Delta x}\frac{dv(x+\Delta x)}{dt}\right]=0 \end{aligned} \qquad [6]$$

$$-\frac{\partial v(x,t)}{\partial x}=L'\frac{\partial i(x,t)}{\partial t}+R'\,i(x,t) \qquad [7]$$

$$-\frac{\partial i(x,t)}{\partial x}=G'v(x,t)+C'\frac{\partial v(x,t)}{\partial t} \qquad [8]$$

Taking the partial derivate with respect to *x* of Eq. [7] and combining with Eq. [8], we arrive at the *Telegrapher's Equation* for a lossy waveguide.[10]

$$-\frac{\partial^2 v(x,t)}{\partial x^2}=-L'G'\frac{\partial v(x,t)}{\partial t}-L'C'\frac{\partial^2 v(x,t)}{\partial t^2}-R'G'\,v(x,t)-R'C'\frac{\partial v(x,t)}{\partial t} \qquad [9]$$

Examination of Eq. [9] in the limit where *G'=L'=0* arrives at the diffusion equation for voltage as follows:

$$\frac{\partial^2 v(x,t)}{\partial x^2}=R'C'\frac{\partial v(x,t)}{\partial t} \qquad [10]$$

These materials have resistivities on the order of 10^{13} to 10^{20} ohm-cm that supports the argument for *G'=0*.[11] However, the argument for *L'=0* is valid as compared to the series resistance *R* in Eq. [7] which is large and dominates the change in voltage between the two circuit nodes. Thus, it is reasonable to neglect *L'* in the calculation. By recognizing that $v(x,t)$ is proportionally related to the surface charge density via the capacitance, we can write Eq. [10] in terms of the surface charge density $\sigma(x,t)$. It is noted that, the solution is found in the rectangular coordinates but applied to cylindrical geometry implying that following derivation is an

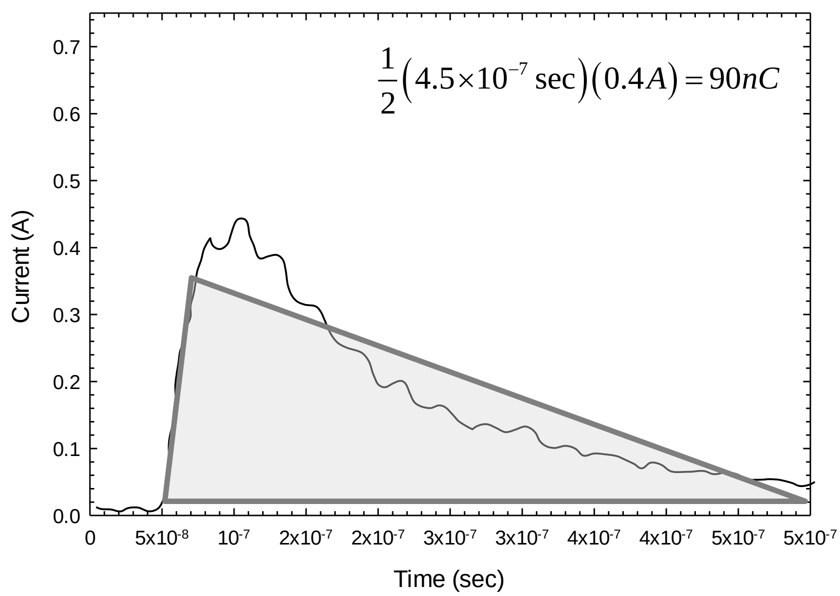

Figure 6: Plot of transient current data from ESD discharge on 50 cm x 50 cm x 6 mm PVC plate charge to a surface density of 10μC/m^2 and discharged into a 20mm diameter grounded metal sphere. Total charge is on the order of 90 nC.

approximation of the true behavior of the system.

Taking the Laplace transform of Eq. [10] leads to the following ordinary differential equation.

$$\frac{d^2\sigma(x,s)}{dx^2} - R'C'\,s\,\sigma(x,s) = -R'C'\sigma_0 \qquad [11]$$

The complete solution of Eq. [11] is the sum of the transient solution (σ_t) and the steady-state solution (σ_{ss}) and has the general form of the following:

$$\sigma(x,s) = \sigma_t + \sigma_{ss} = Ae^{-\sqrt{R'C's}\,x} + Be^{\sqrt{R'C's}\,x} + C \qquad [12]$$

Application of appropriate boundary conditions leads to a solution of Eq. [12]. Since the solution must be bounded at $x \to \infty$, the coefficient B must be zero and the surface charge density in the *s-domain* at $x \to \infty$ leads to $C = \sigma_0 / s$. The final boundary condition is $\sigma(0, s) = 0$. This is due to the *ideal assumption* that a brush discharge on the surface of the polymer initially drains all of the charge from the point-of-contact leaving the surface charge density at the point of the brush discharge equal to zero. Mathematically, this simplifies the development, but it is not exact. In reality, charge is removed but not completely at *x=0*.

The final solution in the *s-domain* to Eq. [11] including this assumption is therefore:

$$\sigma(x,s) = -\frac{\sigma_0}{s} e^{-\sqrt{R'C's}\,x} + \frac{\sigma_0}{s} \qquad [13]$$

Inverting the Laplace transform leads to the following relationship in the time domain.

$$\sigma(x,t) = -\sigma_0 \left(erfc\left(\sqrt{\frac{R'C'}{4}} \frac{x}{\sqrt{t}} \right) - 1 \right) = \sigma_0 \; erf\left(\sqrt{\frac{R'C'}{4}} \frac{x}{\sqrt{t}} \right) \qquad [14]$$

Examination of Eq. [14] implies that we have no confirmable analytical approach to determining the value of the diffusion constant $\sqrt{R'C'}$. Instead, we are compelled to declare the constant an arbitrary parameter and fit Eq. [14] to published data.[12] An order of magnitude correct value for the diffusion constant that results is $R'C' = 2 \times 10^{-3} \; {}^{s}\!/\!{}_{m^2}$.

Figure 5 is a plot of the calculated response from Eq. [14] compared to data obtained from various literature sources. The value of $R'C'=2x10^{-3}\ s/m^2$ is found by fitting the data from Horenstein to Eq. [14]. This data was measured by charging a sample of PVC to -50 μC/m^2 and then discharging it one time using a probe sphere of 30 mm in diameter. Various other sources were then compared to the model with the fit value for overlay of the results.[6, 13,14,15] The amplitudes were normalized due to variation in the initial surface charge density in each of the experiments. General agreement is observed in the width of the charge "crater" measured in the three experiments as well as for the calculation. Since the value of *R'C'* was obtained from only Horenstein, this implies that the other independent measurements are consistent with our model.

The total time window during which the discharge is allowed to operate is t_0 and considering the spatial component *x* only, we can infer a standard radius of charge depletion from the function Eq. [14]. This is appropriate since a review of published results limits the total measurement window to less than 0.5 μs for virtually all of the data reported.[6,12,14] If we arbitrarily define the complete charge depletion region as being within 90% of the final value, then the value of *x* is found to be ~40 mm which is consistent with the measured data and the previously postulated standard radius of 45 mm.

This approach to determining the "standard area" appears arbitrary as Eq. [14] is a continuous function of time and therefore will change over its entire defined values of $0 \leq x \leq \infty$ and $0 \leq t \leq \infty$. However, it must be remembered that the discharge from the polymer surface is not a continuous

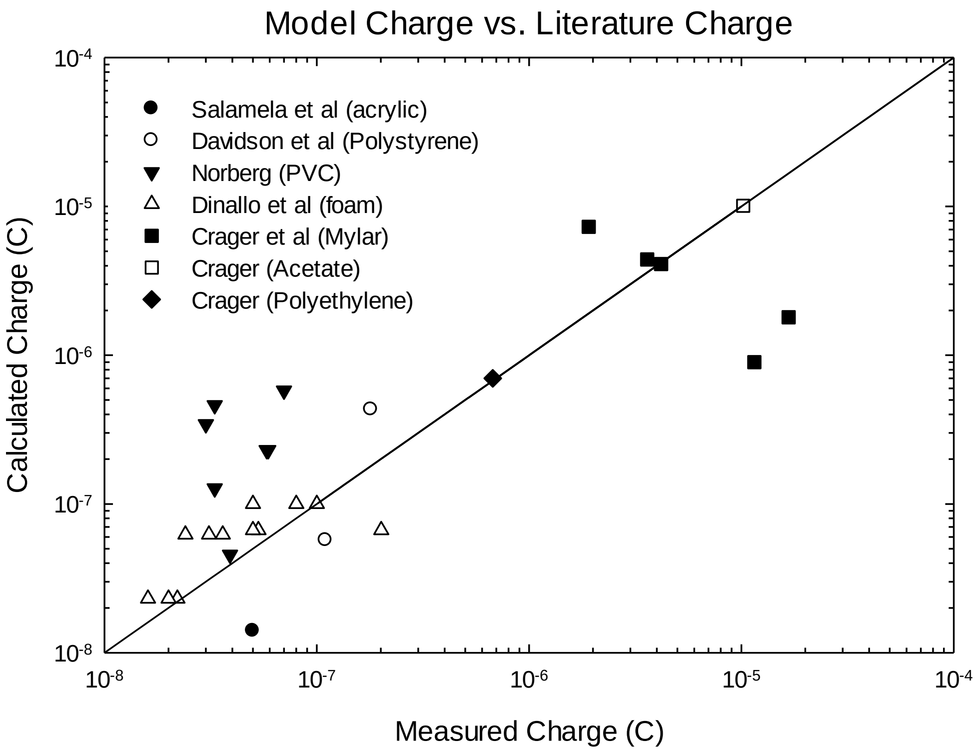

Figure 7: Plot of calculated charge vs. measured charge for several ESD experiments reported in literature from low-conductivity polymers using 10 mm radius grounded electrodes. Data reported for Norberg assumes a maximum surface charge density of 10 μC/m^2. Norberg calculations were all made with a reduced average of 5 μC/m^2. Solid line represents perfect agreement between model and experiment. Data from Crager assumes a uniform *d_m* of 2mm.

function of time in space and will cease when the electric field gradient is smaller than the breakdown field in air as described above. Thus, any of our results are only a useful approximation.

An approximation of the total charge transferred (Q_0) is inferred from Eq. [4] as the following:

$$Q_0 = \varepsilon_0 \left(1 + \frac{\kappa d_m}{d_p + \kappa d_g} \right) \frac{V_f}{d_m} \Delta A \qquad [15]$$

The transfer efficiency is a function of the parameter d_g and has been empirically determined in the literature for polystyrene.[6] This data is shown in Figure 3 and can be fit to an arbitrary equation of the form:

$$T(d_g) = T_0 + A\left(1 - e^{-bd_g(mm)}\right) \qquad [16]$$

The parameters T_0*=6.2%, A=59.6%, and b=0.0349/mm* are found by applying a non-linear least squares fit to the data shown in Figure 3. The plot of Figure 3 implies a variable parameter to our empirically determined standard area (ΔA) of Eq. [15]. Thus, the total charge that is transferred will be corrected to the following form:

$$Q_o' = \varepsilon_0 \left(1 + \frac{\kappa d_m}{d_p + \kappa d_g}\right) \frac{V_f}{d_m} \Delta A \times \frac{T\left(d_g\right)}{100} \qquad [17]$$

In Eq. [17], Q_o' is the corrected total charge from the polymer to the load due to the brush discharge.

Validation

In order to validate the model for the total charge, transient data of current vs. time was found from several sources and the total charge extracted by means of a graphical integral on the data. An example is given in Figure 6.[16] Similar data were extracted and analyzed from other sources.[6, 8, 9, 17, 18] Figure 7 plots the calculated charge compared to the measured charge and illustrates model agreement with published measurements to within an order of magnitude. The data of Figure 7, except for the Dinallo data, is limited to measurements with spark lengths of less than 3 cm for ESD measurements using charged polymer sheets with 10 mm radius grounded electrodes for discharge. Dinallo *et al's* data was taken by extracting charge via 50 mm diameter Cu disk placed in intimate contact (d_m<1 mm) with the polymer and the total charge transferred measured via the voltage on a fixed 100 pF capacitor. Salamla, Dinallo, and Davidson report data measured under controlled environmental conditions of relative humidity less than 35%. Relative humidity less than 35% has been shown to have minimal effect on surface conductivity in polymers. The relative humidity for the Norberg data is not reported but is assumed to be greater than 40% which leads to the overestimate of charge consistently observed in that data set.[19] The solid line represents perfect agreement of the model with measurement.

Examination of Figure 7 illustrates that the model tends to overestimate the amount of charge transferred from the polymer surface to the electrode. This is a favorable bias in the model as it returns a conservative estimate of the charge. The subsequent calculations based on the model will then favor a more robust reliable design that is less susceptible to an ESD event whose total charge is above the statistical mean. Thus, Figure 7 validates the "source term" found in Eq. [17] for further calculation of the response due to ESD from polymers.

CIRCUIT MODEL

If we consider the following circuit as a physical model of the charge storage and delivery mechanism from a polymer (Figure 8), we can infer a Thévenin equivalent circuit that can be represented in the *s-domain* as a quotient of polynomials. The *s-domain* or Laplace transform approach to the solution of a multi-order differential equation has the advantage of providing both a steady-state (principle) solution and a transient (complementary) solution to the equation. Electrostatic discharge by its very nature is a transient event and thus requires such an approach.

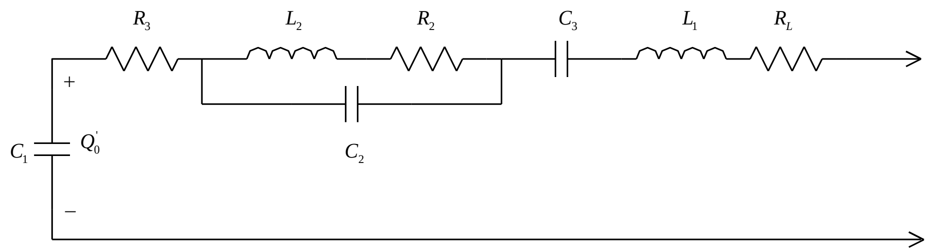

Figure 8: Equivalent circuit model of ESD from a polymer sheet charged to a surface voltage that provides an equivalent Q_o' as found in Eq. [17]. A physical description of the individual elements is given in the text.

Rationale

The discharge of surface immobile charge from a non-conducting sheet can be described as a series of surface discharges that propagate by breakdown of air from an element of charge to an adjacent element of charge. For example, if a probe is brought into proximity to a uniformly charged surface and a small fixed region of charge is discharged into the probe, there is now a non-uniformity in the charge density of the surface that will trend toward becoming uniform.

If the surface was a conductor, then all of the mobile charge would readjust its location to re-stabilize the system. However, for a low-conductivity polymer where the charge is essentially immobile, the only path to move the charge is through breakdown of either the air or the polymer. Since, the polymer generally has a much higher breakdown potential, the charge will move through the air provided that the electric field is greater than the breakdown potential of air (3 MV/m).

When charge moves to the probe, the electric field between adjacent differential charge areas becomes large and continues to breakdown until stability is achieved.[9] This discretized process more resembles a digital circuit than an analog circuit. However, we wish to simulate this process using an analog circuit that can be potentially constructed and used as a laboratory test instrument. Thus, we propose the circuit of Figure 8 as an analog simulation of a surface discharge from a low-conductivity polymer surface.

In Figure 8, C_1 represents the total capacitance of the sheet over the standard area (ΔA) described above and is charged to a total charge Q_o' according to Eq. [17] which is a function of the surface potential of the material. Charge Q_o' is then allowed to dissipate via R_3 into an oscillator circuit comprised of components R_2, L_2, and C_2. This tank circuit is designed to simulate the oscillatory behavior of the sequential discharge of the ions from differential area to differential area as described above. The tank circuit energy is then coupled via C_3 to the resistance R_L through a path with an equivalent inductance of L_1. R_3 is the resistance of the discharge between the surface and the conducting probe. C_3 is the capacitance between the charged surface and the probe. L_1 represents the inductance of the path to ground.

The short circuit current (I_{sc}) and the open circuit voltage (V_{oc}) were found to generate an Thévenin equivalent circuit (Figure 9). We write the following relationship in the *s-domain* for the voltage across RL with the circuit end (Figure 8) shorted.

$$V_{out}(s) = \frac{v_o C_1 R_L C_3 (s^2 C_2 L_2 + s C_2 R_2 + 1)}{\begin{gathered} s^4 L_1 L_2 C_1 C_2 C_3 + s^3 \left(L_2 C_1 C_2 C_3 \left(R_L + R_3 \right) + R_2 L_1 C_1 C_2 C_3 \right) + \\ s^2 \left(L_1 C_1 C_3 + L_2 C_1 C_3 + L_2 C_1 C_2 + L_2 C_2 C_3 + C_1 C_2 C_3 R_2 \left(R_L + R_3 \right) \right) + \\ s \left(R_2 C_1 C_2 + R_2 C_2 C_3 + R_2 C_1 C_3 + R_L C_1 C_3 + R_3 C_1 C_3 \right) + \left(C_1 + C_3 \right) \end{gathered}} \quad [18]$$

Rewriting Eq. [18] for simplicity yields the following quotient of polynomials:

$$\begin{aligned} V_{out}(s) &= v_o C_1 R_L \frac{f(s)}{g(s)} \\ f(s) &= C_3 (s^2 C_2 L_2 + s C_2 R_2 + 1) \\ g(s) &= s^4 L_1 L_2 C_1 C_2 C_3 + s^3 \left(L_2 C_1 C_2 C_3 \left(R_L + R_3 \right) + R_2 L_1 C_1 C_2 C_3 \right) + \\ &\quad s^2 \left(L_1 C_1 C_3 + L_2 C_1 C_3 + L_2 C_1 C_2 + L_2 C_2 C_3 + C_1 C_2 C_3 R_2 \left(R_L + R_3 \right) \right) + \\ &\quad s \left(R_2 C_1 C_2 + R_2 C_2 C_3 + R_2 C_1 C_3 + R_L C_1 C_3 + R_3 C_1 C_3 \right) + \left(C_1 + C_3 \right) \end{aligned} \quad [19]$$

Examination of Eq. [18] implies a straight forward relationship between the surface voltage (v_o) of the low-conductivity material and the output voltage across R_L. However, a difficulty arises

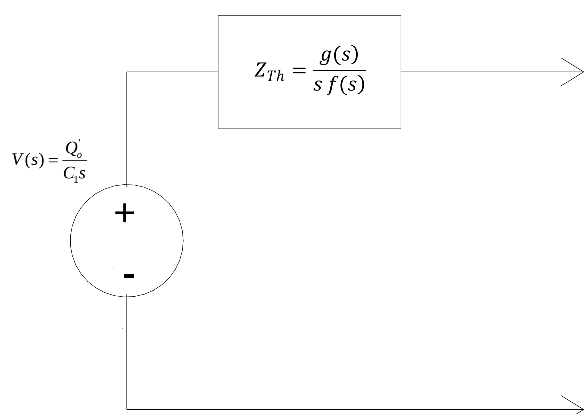

Figure 9: Illustration showing Thévenin equivalent of the low-conductivity surface ESD simulation circuit where *f(s)* and *g(s)* are defined in Eq.[19].

with respect to the true value of v_o and the true value of C_1 that would not occur if the charge resided on a conducting surface. In that case, the capacitance is easily determined via geometrical considerations.

By examining the data of Figure 11 and ignoring the high–frequency modulation, we can imply the general form of the response of an ESD event as a decaying exponential of the form of $\left(I_o e^{-t/C_1 R_L}\right)$. Timing measurements can be used to roughly estimate the RC time constant ($R_L C_1$ in Figure 8), but cannot infer the value of the individual components without defining one or the other. From the literature, it has been reported that a spark resistance can be on the order of 1-4 kΩ implying that choice of a representative value can lead to a value of C_1.[20] The choice of C_1

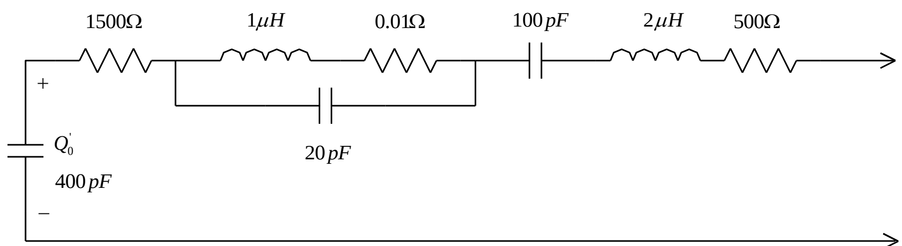

Figure 10: Proposed circuit model of ESD from a polymer sheet charged to a surface voltage that provides an equivalent Q_o' as found in Eq. [17]. Thévenin equivalent in the *s*-domain is given in Eq. [21].

leaves the value of v_o in question as the region of discharge is not well behaved eliminating a geometrical determination of v_o as would be possible with a system of mobile charges in a conductor.

The solution to this difficulty arises by recognition that the product $v_o C_1$ is the total charge that is available for transfer from the film to ground. Thus, substitution of Eq. [17] into Eq. [19] and division by R_L leads to an expression for the *s-domain* short circuit current.

$$I_{sc}(s) = \varepsilon_0 \left(1 + \frac{\kappa d_m}{d_p + \kappa d_g}\right) \frac{V_f}{d_m} \Delta A \times \frac{T(d_g)}{100} \times \frac{f(s)}{g(s)} = Q_0' \times \frac{f(s)}{g(s)} \qquad [20]$$

This allows us to write a Thévenin equivalent circuit for the ESD discharge as shown in Figure 9.

$$\begin{aligned} Z_{Th} &= \frac{g(s)}{sf(s)} \\ V(s) &= \frac{Q_o'}{C_1 s} \end{aligned} \qquad [21]$$

Numerical Approach

Examination of the Thévenin equivalent (Eq. [21]) and the form of Eq. [18] implies the need for a numerical method of inverting the Laplace transform into the time domain. An analytical solution of the inverse Laplace transform of Eq. [18] requires the factorization of the denominator of Eq. [18] which is at a minimum a forth order polynomial and quickly becomes problematic. Thus, we resort to the application of the numerical inverse Laplace transform algorithm described by Moreno and Ramirez.[21]

As a reminder, the analytical Laplace transform pair is given by the following relationships:

$$F(s) = \int_0^\infty f(t)e^{-st}dt \qquad [22]$$

$$f(t) = \frac{1}{2\pi j}\int_{s=\alpha-j\infty}^{s=\alpha+j\infty} F(s)e^{st}ds \qquad [23]$$

Where $s = \alpha + j\omega$ is called the complex frequency, *f(t)* is a well behaved function of time, and *F(s)* is the Laplace transform of *f(t)* as defined above. Our application requires the inverse transform (Eq. [23]) and an appropriate method to numerically calculate the solution.

If we rewrite Eq. [22] as the following recognizing that α is a large positive real number and ω is a frequency variable, we obtain:

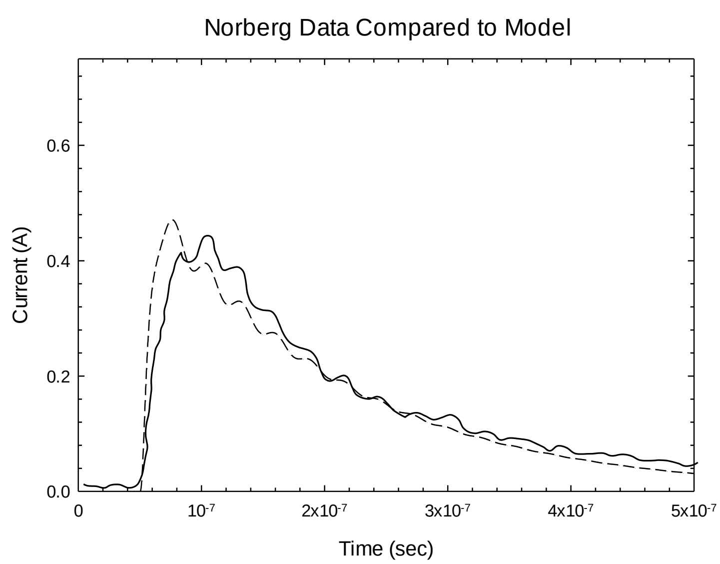

Figure 11: Plot of transient discharge data from literature (black line) compared to solution of the model of Eq. [18] (dashed line). In the circuit, R2=0.01Ω, R3=1500Ω, C1=400 pF, L1=2 μH, R_L=500Ω, C2=20 pF, L2=1 μH, C3=100 pF, and v_o=28kV. The voltage is inferred from the published charge density of 10 μC/m^2. Solution is corrected for time constants in the measurement apparatus.

$$F(s)=\int_0^{\infty} f(t)e^{-(\alpha+j\omega)t}dt=\int_0^{\infty}\left[f(t)e^{-\alpha t}\right]e^{-j\omega t}dt \qquad [24]$$

$$f(t)=\frac{e^{\alpha t}}{2\pi}\int_{-\infty}^{\infty} F(s)e^{j\omega t}d\omega \qquad [25]$$

Careful examination of Eq. [24] indicates that the Laplace transform of *f(t)* is equivalent to the Fourier transform of the damped function $f(t)e^{-\alpha t}$. Thus, the inverse Laplace transform of *F(s)* can be found by treating the *s*-domain function as an inverse Fourier transform with an appropriate exponential function $e^{\alpha t}$. The stipulation on this approach is that α must be large enough to be to the right of all of the poles of *F(s)* which allows the contour integral to surround all of the poles.[21,22]

The convenience of this approach is that fast Fourier transform algorithms are available in packages such as Matlab allowing this calculation. However, judicious choice of the value of α is required for the results to be valid. The method of Wedepohl was chosen so that α is cast in terms of the number data samples (N) and the total period of the calculation (*T*).[23]

$$\alpha=\frac{\ln\left(N^2\right)}{T} \qquad [26]$$

A sample listing of a Matlab program to accomplish the inverse Laplace transform of the function (Eq. [20]) using the values of Figure 10 is given in Appendix A.

Now all of the tools are in place to test our algorithm. A comparison of this result with published transient results from samples of PVC excited by way of mechanically rubbing the surface using cat fur to charge densities on the order of 10 $\mu C/m^2$ is shown in Figure 11.[16]. The calculated data of Figure 11 are corrected for the rise time of the Rogowski coil (4.7 ns) and the input of the

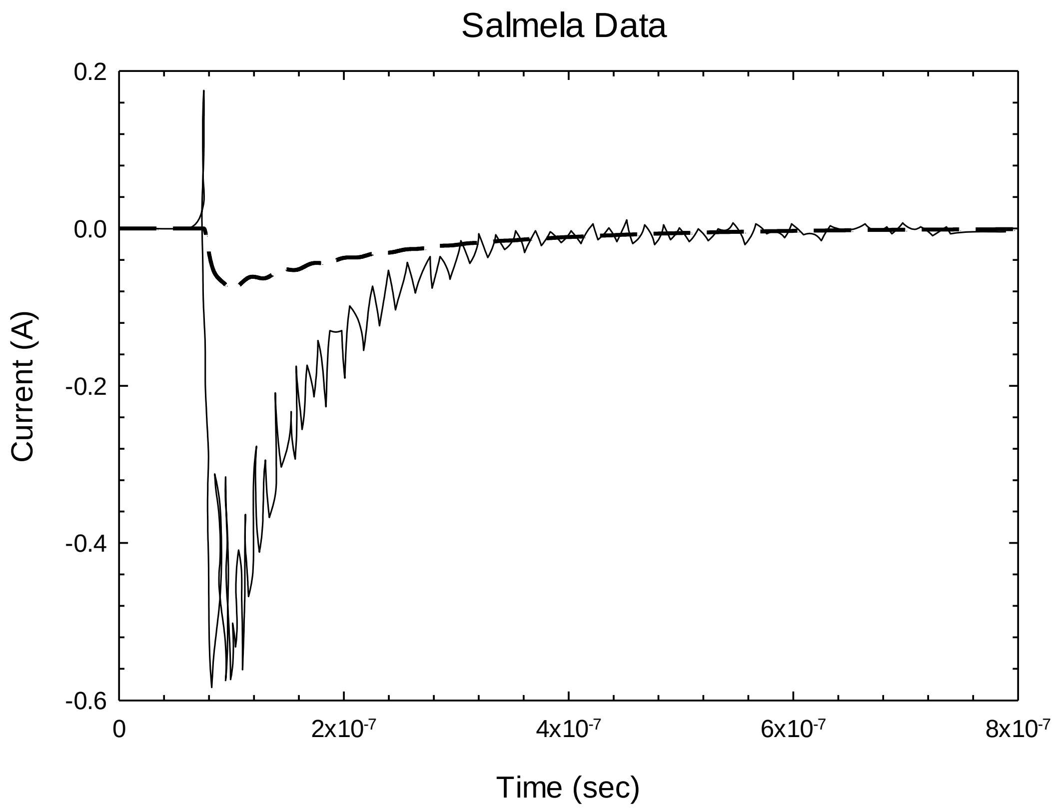

Figure 12 Plot of transient discharge data from literature (thin line) compared to solution of the model of Eq. [18]. In the circuit, R2=0.01Ω, R3=1500Ω, C1=400 pF, L1=2 µH, R_L=500Ω, C2=20 pF, L2=1 µH, C3=100 pF, and v_o=-40kV. Solution is corrected for time constants in the measurement apparatus (thick dashed line). Data agrees to within about a factor of 5 which is consistent with the calculated charge.

digitizer (50 Ω and 30 pF). Figure 11 illustrates good agreement for the model compared to the data of Norberg.[16] The model was also compared to the results of Salmala[17] as shown in Figure 12 and has an error of about a factor of 5 as predicted by the deviation from the predicted value for this data in Figure 7. This indicates that a standard model for ESD should have a standard initial charge that is large enough to bound the potential cases that have been studied. The final model is the calculated response from the data of Dinallo for which there is no published transient data (Figure 13). However, the variation demonstrates the uncertainty of the ESD from polymer problem.

3: FINAL MODEL

Based in the studies above, we propose Figure 10 as a standard simulation circuit for ESD events

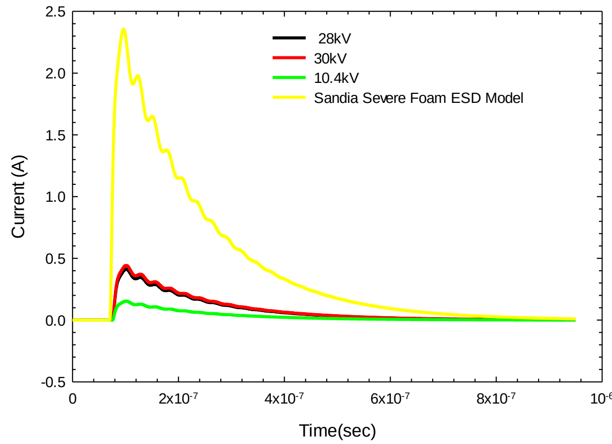

Figure 13: Plot of three simulations from the Dinallo[8] data showing the variation in the response that can occur in the charging and the ESD from selected polymers. As illustrated, factors of 4 to 5 difference in peak amplitude under identical experimental situations are possible. Data are compared to the Sandia Severe Foam ESD Model.

from the surface of polymer films. In Figure 10, Q_0' is the total charge available for transfer and is compensated for the transfer efficiency as described in Eq. [17]. The data are fit to the literature data to the function until reasonable agreement with the transient data is achieved to obtain the values of the passive components.

As described above, the calculation of the charge available for transfer is dependent on the geometry of the polymer as well as its physical size and electrical properties. However, for this model to be applicable, we would like to bound the solution by choosing an appropriate value of Q_o that incorporates the worst reasonable case conditions possible in Eq. [20] as the initial charge on C_1. Figure 7 suggests that the maximum reasonable charge possible on various polymers is on the order of $2x10^{-6}$ C (data points from mechanical charging are below this value). Thus, we propose the model of Eq. [20] where the initial charge is 2×10^{-6} C and the component values chosen in Figure 10 are the passive values for a bounded ESD from foam components. A plot comparing the short circuit current from discharge of foams charged to several surface potentials compared to the results from this charge condition is given in Figure 13. The values provide an upper bound with a safety margin on the order of 5. This data is labeled the *Sandia Severe Foam ESD Model*.

4: CONCLUSIONS

In conclusion, we have developed an analog circuit model to simulate an ESD pulse that is charged to a 2µC surface charge as a bounding condition for ESD from foam components (Sandia Severe Foam ESD Model). The model simulates the major features of measured pulses found in the literature including the decaying exponential envelope modulated with a fast oscillation. The model is based on the premise that charge from polymers will migrate from regions of high charge density to regions of low charge density in a discretized manor that relies on breakdown of the air. Values of circuit elements are obtained by fitting literature data to the model. The time response of the model is found by numerical inversion of the Laplace transform of the circuit.

Sandia National Laboratories is a multi-program laboratory managed and operated by Sandia Corporation, a wholly owned subsidiary of Lockheed Martin Corporation, for the U.S. Department of Energy's National Nuclear Security Administration under contract DE-AC04-94AL85000.

5: APPENDIX A: SAMPLE LAPLACE INVERSE PROGRAM

```
%MatLab program to find short-circuit current for ESD from polymer
clear all;
% Laplace data;
T=1000*1e-9; %simulation interval interval (ns)
N=4096*2;
error=0.0001;
dw=pi/T;

dt = T/N; %sampling interval

% choose alpha;
alpha = log(N^2)/T;
t=dt*[0:N-1];
m=[1:2:2*N];
s=c+1i*m*dw;
n=[0: N-1];
Cn=(N*2*dw/pi)*exp(alpha*dt+1i*pi/N).^n;


%ESD Circuit Values found from fitting data of Norberg Data

R2=.01;%ohms
R3=1500; %ohms
C1=.4E-9; %Farads
L1=2000e-9; %Henry
RL=500; %ohms
C2=20e-12; %Farads
L2=1e-6; %Henry
C3=100e-12; %Farads

epsilon=8.85e-12; %F/m
polymer_thickness=0.006; %m
measurement_height=0.01; %m
height_ground=0; %m
standard_area=6.4e-3; %m^2
dielectric_const_polymer=3; %unitless
Vfoam=28000; %V 10uC/m^2 charge density at infinite distance from GND plane

Transfer_correction=0.062+0.596*(1-exp(-34.9*measurement_height))
%Transfer Function is s-domain
fs=s.^2*C2*C3*L2+s*C2*C3*R2+C3;
```

```
gs=s.^4*L1*L2*C1*C2*C3+s.^3*(L2*C1*C3*C2*RL+L2*C1*C3*C2*R3+L1*C1*C2*C3*R2
)+s.^2*(L1*C1*C3+C1*L2*C3+C1*C2*C3*R2*(RL+R3)+C1*C2*L2+C2*C3*L2)+s*(C1*C2
*R2+C2*C3*R2+C1*C3*R2+C1*C3*RL+C1*C3*R3)+(C1+C3);
Qo=Vfoam/measurement_height*epsilon*(1+dielectric_const_polymer*measurement_height/(p
olymer_thickness+dielectric_const_polymer*height_ground))*standard_area*Transfer_correctio
n
Fs1=Qo*fs./gs.*exp(-s.*tau);%correction for time delay
Fs2=Fs1./(1+s.*Rscope*Cscope);%correction for scope input impedance
Fs=Fs2./(s.*Tcoil+1); %correction for rise time in sampling coil


% Window function to reduce edge ringing;
sigma=0.5*(1+cos(0.5*pi*m/N)); %Hanning window function;

% function in the time domain through NLT;

Fs=Fs.*sigma; %comment this line to make it without window function;

ftd=ifft(Fs);
ftd=real(Cn.*ftd);

%plotting;
Np=floor(N*.95);

figure, plot(t(1:Np), real(ftd(1:Np)));
```

6. REFERENCES

[1] Liou, J. J., *Electrostatic Discharge (ESD) Protection of RF Integrated Circuits*, 2012 IEEE Asia Pacific Conference on Circuits and Systems, Kaohsiung, Taiwan, (2012) pp 460-462.

[2] Gerardin, S., Griffoni, A., Tazzoli, A., Cester, A., Meneghesso, G., Paccagnella, A.; *Electrostatic Discharge Effects in Irradiated Fully Deplete SOIMOSFETs With ultra-Thin Gate Oxide*, IEEE Transactions on Nuclear Science, **54**, 6, (2007), pp. 2204-2209.

[3] Bicleanu, P., Nicuta, A. M., Bargan, L., Salceanu, A., Postolache, O.; *Protective Circuitry Developments Related to MOSFET Protection Setup to the Occurrence of Electrostatic Discharge Phenomenon*, 2012 International Conference and Exposition on Electrical and Power Engineering, Iasi, Romania, (2012) pp. 723-727.

[4] Mateo-Velez, J. C., Inguimbert, V., Toyoda, K., Payan, D., Balcon, N., *Time-Resolved Spectroscopy of Electrostatic Discharge and Secondary Arc Plasma on Spacecraft Solar Array*, IEEE Transactions on Plasma Science **40,** 2, (2012) pp 359-367.

[5] Jackson, J. D., *Classical Electrodynamics*, 2nd Ed., John Wiley and Sons, New York, New York, (1975) pp. 17-19.

[6] J. L. Davidson, T. J. L., Williams, A. G.T. J., Bailey, A. G. L.., Hearn;, G. L.; *Characterisation of the Electrostatic Discharges from Insulating Surfaces*, Journal of Electrostatics, **50-51,** (2001) pp), pg. 374-380.

[7] Castle, G. S. P., Inculet, I. I., *The Electrostatic Fields and Discharge hazards of Insulating Sheets Close to a Conductor: A Review*, IEEE Transactions on Industry Applications, **33**, 1, Jan./Feb. (1997), pp. 274-278.

[8] Dinallo, M. A., Howard, K. R., Morris, M. E., B61-3/3/10 and B61-7/11 Dielectric Polymer Component Contact Electrostatic Discharge Measurements: Using War Reserve Pristine Foams to Contact Internal B61 Cable Connectors in a Low Relative Humidity Environment, SAND2008-3882, Sandia National Laboratories, Albuquerque, NM, July 2008.

[9] Crager, J. C., HorensteinHorenstin, M. N., Distributed Parameter Model for Computing Energy Dissipation in Brush-Type Electrostatic Discharge, J. of Electrostatics, **63**, (2005), pp. 239-247.

[10] S. Karni, W. J. Byatt, *Mathematical Methods in Continuous and Discrete Systems*, Holt, Rinehart and Winston, New York, New York, (1982), pp. 143-144.

[11] http://www.pvc.org/en/p/electrical-insulation-characteristics (2014)

[12] Horenstein, M. N. A Simulation Model for understanding Propagating Brush Discharges: Comparison of Theory and Experiments, IEEE Transactions on Industry Applications, **47**, 1, Jan./Feb. 2011.

[13] Horenstein, M. N.; *Review of Progress in Understanding Propagating Brush Discharges*, 42nd Annual Meeting of the IEEE-Industry-Applications-Society Location: New Orleans, LA, (2007) pp. 1093-1097

[14] L. Mueller, K. Feser; *Experimental and Theoretical Investigation of Surface Discharges for Charged Dielectric Materials*, 2002 Annual Report Conference on Electrical Insulation and Dielectric Phenomena, Cancun Mexico, (2002) pp. 122-125.

[15] Davidson, J. L., Williams, T. J., Bailey A. G.; *Electrostatic Discharges Between Charged Insulators and Grounded Spheres,* Journal of Electrostatics, **56**, (2002), pg. 29.

[16] Norberg, A; *Modeling Current Pulse Shape and Energy in Surface Discharges*, IEEE Transactions on Industry Applications, **28**, 3, May/June 1992, pp. 498, 503.

[17] Salmela, H., Paasi, J., Kalliohak, T., Fast, L., Measurements of Air Discharges from Insulating, Electrostatic Dissipative and Conducting Materials with Different ESD Probes, J. of Electrostatics **63,** (2005), pp. 539-544.

[18] Landers, E. U., Distribution of Charge and Fieldstrength Due to Discharge from Insulating Surfaces, J. of Electrostatics, **17**, (1985), pp. 59-68.

[19] Gibson, N., Lloyd, F. C., *Incendivity of Discharges from Electrostatically Charged Plastics*, Brit. J. Appl. Phys., **16**, (1965), pp. 1619-1631.

[20] Norberg, A., Szedenik, N., Lundquist, S.; *On the Pulse Shape of Discharge Currents,* J. of Electrostatics, **23,** (1989), pp. 79-88.

[21] Moreno, P., Ramirez, A., *Implementation of the Numerical Laplace Transform: A Review,* IEEE Transactions on Power Delivery, **23**, 4, (2008), pp. 2599-2608.

[22] Karni, S., Byatt, W. J., *Mathematical Methods in Continuous and Discrete Systems*, Holt, Rinehart and Winston, New York, pp. 78-107.

[23] Wedepohl, Power System Transients: Errors Incurred in the Numerical Inversion of the Laplace Transform, in Proc. 26th Midwest Symp. Circuits Systems, Aug. 1983, pp. 174-178.

DISTRIBUTION

[

5	MS0382	M. T. Kerschen	2152
1	MS0382	P. D. Hoover	2152
1	MS0382	H. D. Radloff	2152
1	MS0382	D. R. Weiss	2127
1	MS0382	J. L. Sichler	2153
1	MS0382	C. Eiting	2153
1	MS0382	M. A. Polosky	2153
1	MS0382	K. J. Schwing	2152
1	MS0382	L. S. Weichman	2152
1	MS0386	J. C. Fonseca	2128
1	MS0386	M. A. Yaklin	1557
1	MS0386	A. T. Murray	5784
1	MS0386	S. A. Sanchez	2159
1	MS0386	K. R. Pohl	2159
1	MS0405	K. O. Merewether	0434
1	MS0892	L. G. Stotts	1716
1	MS1078	W. L. Hermina	1710
1	MS1152	M. A. Dinallo	1353
1	MS1152	R. K. Howard	1353
1	MS1209	J. B. Wirth	5956
5	MS1425	K. B. Pfeifer	1716
1	MS0899	Technical Library	9536 (electronic copy)
1	MS0115	OFA/NFE Agreements	10012

Sandia National Laboratories